Author Contributions:

Conceptualization: Yang Song, Josep Penuelas, Lixin Wang
Formal analysis: Yang Song
Funding acquisition: Xiuliang Jin
Investigation: Yang Song
Methodology: Yang Song, Josep Penuelas, Philippe Ciais, Songhan Wang, Yao Zhang, Pierre Gentine, Matthew F. McCabe, Lixin Wang
Project administration: Zhenong Jin, Chaoyang Wu, Xiuliang Jin
Resources: Lixin Wang
Software: Yang Song
Supervision: Josep Penuelas, Lixin Wang, Zhenong Jin, Chaoyang Wu, Xiuliang Jin

Recent Water Constraints Mediate the Dominance of Climate and Atmospheric CO_2 on Vegetation Growth Across China

Yang Song[1,2], Josep Penuelas[3,4], Philippe Ciais[5], Songhan Wang[6], Yao Zhang[7,8], Pierre Gentine[9], Matthew F. McCabe[10], Lixin Wang[11], Xing Li[12], Fei Li[13], Xiaoping Wang[14], Zhenong Jin[15], Chaoyang Wu[16], and Xiuliang Jin[1,2]

[1]Institute of Crop Sciences, Chinese Academy of Agricultural Sciences/Key Laboratory of Crop Physiology and Ecology, Ministry of Agriculture, Beijing, China, [2]National Nanfan Research Institute (Sanya), Chinese Academy of Agricultural Sciences, Sanya, China, [3]CSIC, Global Ecology Unit, CREAF-CSIC-UAB, Barcelona, Spain, [4]CREAF, Cerdanyola del Vallès, Barcelona, Spain, [5]Laboratoire des Sciences du Climat et de l'Environnement, LSCE/IPSL, CEA-CNRS-UVSQ, Université Paris-Saclay, Gif-sur-Yvette, France, [6]College of Agriculture, Nanjing Agricultural University, Nanjing, China, [7]Sino-French Institute for Earth System Science, College of Urban and Environmental Sciences, Peking University, Beijing, China, [8]Institute of Carbon Neutrality, Peking University, Beijing, China, [9]Department of Earth and Environmental Engineering, Columbia University, New York, NY, USA, [10]Hydrology, Agriculture and Land Observation Laboratory, Division of Biological and Environmental Science and Engineering, King Abdullah University of Science and Technology, Thuwal, Saudi Arabia, [11]Department of Earth and Environmental Sciences, Indiana University Indianapolis, Indianapolis, IN, USA, [12]Research Institute of Agriculture and Life Sciences, Seoul National University, Seoul, South Korea, [13]Grassland Research Institute, Chinese Academy of Agricultural Sciences, Hohhot, China, [14]College of Natural Resources and Environment, Northwest A&F University, Yangling, China, [15]Department of Bioproducts and Biosystems Engineering, University of Minnesota, St. Paul, MN, USA, [16]The Key Laboratory of Land Surface Pattern and Simulation, Institute of Geographic Sciences and Natural Resources Research, Chinese Academy of Sciences, Beijing, China

Abstract Multiple lines of evidence confirm a widespread increase in vegetation growth across China over the past few decades. The relationship between vegetation growth and water availability is thought to be becoming stronger under climate change, that is, water constraints on vegetation growth have been increasing. However, our understanding of how water constraints have influenced these vegetation greening trends, especially those climate change-driven ones, remains limited. Here, we conduct a comprehensive evaluation of recent water constraints and their implications for vegetation growth in China between 1982 and 2015. By analyzing the spatiotemporal patterns of the relationship between vegetation growth and water availability, we reveal recent water constraints and their changes hidden within an overall greening trend in China. Further analysis demonstrates that two climate change-related categories, defined broadly as "climate" (e.g., air temperature, precipitation, and so on) and "CO_2" (i.e., atmospheric carbon dioxide), have exerted varying levels of importance in regulating vegetation growth across different water constraints. With increasing water constraints, the proportion of the climate-dominated area has significantly risen, while that of the CO_2-dominated area has sharply declined. Our findings highlight that water constraints can mediate the dominance of climate and atmospheric CO_2 on vegetation growth. This has the great potential to exacerbate the uncertainty surrounding current and future sustainable vegetation greening trends.

Plain Language Summary China's vegetation growth has shown a broad increase under climate change and human activities over the past few decades. At the same time, changes in vegetation water demand, terrestrial water availability, and climatic factors are expected to lead to increasing water constraints on vegetation growth. However, whether water constraints have influenced climate change-driven vegetation greening trends remains unclear. In this study, we provide a comprehensive assessment of recent water constraints and their implications for vegetation growth in China between 1982 and 2015. To do this, we analyze the spatiotemporal patterns of the relationship between vegetation growth and water availability to reveal recent water constraints hidden within China's vegetation greening. Further analysis shows that climate and atmospheric CO_2 have exerted varying levels of importance in regulating vegetation growth across different water constraints. With increasing water constraints, more regions become climate-dominated and fewer become CO_2-dominated. Overall, our findings highlight that water constraints can mediate the dominance of

Validation: Yang Song, Josep Penuelas
Visualization: Yang Song
Writing – original draft: Yang Song
Writing – review & editing:
Josep Penuelas, Philippe Ciais,
Songhan Wang, Yao Zhang,
Pierre Gentine, Matthew F. McCabe,
Lixin Wang, Xing Li, Fei Li,
Xiaoping Wang, Zhenong Jin,
Chaoyang Wu, Xiuliang Jin

climate and atmospheric CO_2 on vegetation growth. This will help decision-makers recognize the uncertainty of sustainable vegetation greening trends.

1. Introduction

Since the Industrial Revolution, climate change and direct human activities have shown a significant impact on water, carbon, and energy exchanges between the land surface and the atmosphere across a large part of the planet (Novick et al., 2016; Sellers et al., 1997). Too much or too little water availability can disrupt normal vegetation growth, both for natural and cultivated plants. Although recent studies have shown that global vegetation is greening as a result of elevated atmospheric carbon dioxide (CO_2) concentrations, nitrogen deposition, climate warming, and changes in land-use and land-management at regional and continental scales, this is simultaneously exacerbating water demands on ecosystems to some extent (Fernandez-Martinez et al., 2019; Gonsamo et al., 2021; He et al., 2019; Li, Ryu, et al., 2023; Lu et al., 2016; Penuelas et al., 2017; Zhu et al., 2016). Besides, unpredictable variations in annual terrestrial water storage (TWS) are likely to further heighten the uncertainty in water availability (Hsu & Dirmeyer, 2023; Humphrey et al., 2018; Pokhrel et al., 2021). Terrestrial vegetation growth has encountered considerable water-related challenges over the past decades (Jiao et al., 2021; Penuelas, 2023; Yuan et al., 2019). Global ecosystems are projected to become increasingly vulnerable to droughts associated with climate change in the future (Higgins et al., 2023; Sherwood & Fu, 2014; Wang et al., 2022). As a result, we are obliged to take into account water constraints on vegetation growth when looking at the current phenomenon of the greening of the Earth.

Satellite observations have demonstrated a vegetation greening trend in China since the early 1980s (Chen et al., 2019; Piao et al., 2015). Climate change has extended the active growing season and enhanced photosynthesis, benefiting most vegetation, especially in regions with sufficient water supply (Bastos et al., 2019; Thomas et al., 2016). As a populous country, China has extensively utilized its land for agriculture and forestry, and policy directives such as agricultural intensification and reforestation have contributed to China's greening in recent decades (Bueso et al., 2023; Gerlein-Safdi et al., 2020; Piao et al., 2010, 2020; Tong et al., 2018). However, this large-scale ecosystem productivity increase is believed to have reduced TWS in China, potentially leading to water constraints on vegetation growth, particularly in arid regions and for irrigated croplands (Huang et al., 2023; Li et al., 2021, 2023c; Wang, Xiao, et al., 2020; Yang, Cui, et al., 2023). Despite elevated atmospheric CO_2 concentrations improving water use efficiency, China's vegetation growth is expected to remain highly dependent on water availability (Li et al., 2022; Wei et al., 2023; Zhang et al., 2022). Recent studies underscore the significance of understanding how vegetation responds to water availability, particularly concerning the negative impacts of droughts on ecosystem productivity (Ciais et al., 2005; Li et al., 2020; Zhang, Zhou, et al., 2023; Zhao & Running, 2010), vegetation resilience to drought (Anderegg et al., 2018; Smith & Boers, 2023; Zhang, Liu, et al., 2023), and sustainable vegetation growth under a changing climate (Berg & McColl, 2021; Jiao et al., 2021; Song et al., 2022). For China, whether vegetation greening trends will be sustainable in the face of potentially limited water resources is a matter of great concern for decision-makers.

In this study, we aim to assess how recent water constraints have influenced vegetation growth trends across China over the past three decades. The Normalized Difference Vegetation Index (NDVI) (Pinzon & Tucker, 2014), Leaf Area Index (LAI) (Liu et al., 2012), and Gross Primary Productivity (GPP) (Wang et al., 2021) were used as proxies for vegetation growth to demonstrate the greening of China's vegetated regions. NDVI, LAI, and GPP are three different indicators associated with vegetation growth. The synergistic use of them plays a crucial cross-validation role in studying vegetation dynamics and climate change (Chang et al., 2023; Wagle et al., 2014; Wang, Zhang, et al., 2020; Xie et al., 2019). We also employed proxies for water availability, including the Palmer Drought Severity Index (PDSI) (Abatzoglou et al., 2018), the Standardized Precipitation-Evapotranspiration Index at the 3-month time scale (SPEI03) (Vicente-Serrano et al., 2010), and TWS (Döll et al., 2014). The relationship between vegetation growth and water availability was used to evaluate different water constraints on vegetation growth and to identify water deficit and water surplus regions within China. Moreover, we tracked trends in the relationship between vegetation growth and water availability over time using 10-year moving windows to exhibit any underlying spatiotemporal patterns. Furthermore, we conducted an ensemble of analyses to reveal the implications of recent water constraints for vegetation growth. We used two climate change-related categories, defined broadly as "climate" (including air temperature, precipitation, and so

on) and "CO_2" (i.e., atmospheric CO_2), to investigate potential shifts in their dominant roles on vegetation growth across different water constraints. Land use change, nitrogen deposition, management practices, and so on were considered in an additional category, "other factors" (Chen et al., 2019; Piao et al., 2015; Zhu et al., 2016). To enhance the robustness of our core findings, we applied partial correlation, machine learning, and multi-scenario modeling simulations to achieve the attribution analysis, respectively (Fernandez-Martinez et al., 2019; Hutley et al., 2022; Jiao et al., 2021; Obermeier et al., 2021).

2. Materials and Methods

2.1. Satellite Observation Data

The third-generation Global Inventory Monitoring and Modeling System (GIMMS) NDVI data (GIMMS NDVI3g, Version 5) (Pinzon & Tucker, 2014), the consistent long-term global LAI product (GLOBMAP LAI, Version 3) (Liu et al., 2012), and the long-term GPP data set based on NIRv (GPP_{NIRv}, Version 2) (Wang et al., 2021) were used in this study as proxies for vegetation growth during the 1982–2015 period. We used the three different proxies for vegetation growth for cross-validation with the aim of reinforcing the robustness of our core findings. All the satellite observation data were aggregated to a 0.05° × 0.05° spatial resolution and a monthly temporal resolution using the nearest neighbor resampling method and the mean value composite method, respectively. We calculated their mean growing-season values for April to October as the annual vegetation growth indicators. The maximum value composite method was used to obtain the annual peak growing-season values to test the robustness of using a fixed-length growing season.

2.2. Eddy-Covariance Flux Tower-Based GPP Data

The eddy-covariance flux tower-based GPP data from ChinaFLUX were used to evaluate the robustness of our satellite-based vegetation growth trend analysis. Limited by the low availability of open-source eddy-covariance flux tower data in China, only the nine sites with at least 6 years of valid GPP estimates during our study period were selected for this study, that is, Xishuangbanna (BNF, forest, 2003–2010), Yucheng (YCA, cropland, 2003–2010), Changbaishan (CBF, forest, 2003–2010), Dinghushan (DHF, forest, 2003–2010), Damxung (DXG, grassland, 2004–2010), Haibei (HBG1, grassland, 2003–2010; HBG2, grassland, 2004–2009), Inner Mongolia (NMG, grassland, 2003–2010), and Qianyanzhou (QYF, forest, 2003–2010). Since these data were short-term, more analyses based on them could be not statistical significant. After attempting to do so, we discarded all the other analyses using eddy-covariance flux tower-based data except for the trend analysis.

2.3. Dynamic Global Vegetation Models

We used the monthly GPP data estimated by dynamic global vegetation models (DGVMs) from the TRENDY project (TRENDYv8, Version 8) (Friedlingstein et al., 2019). The three DGVMs with a fine spatial resolution were selected for this study, that is, ORCHIDEE (Krinner et al., 2005), SDGVM (Walker et al., 2017), and VISIT (Kato et al., 2013). The GPP outputs were derived from the S0 (pre-industrial climate and CO_2), S1 (pre-industrial climate and observed CO_2), S2 (observed climate and CO_2), and S3 (observed climate and CO_2 and land use/land cover) simulation scenarios (Fernandez-Martinez et al., 2019; Friedlingstein et al., 2019). We resampled the simulated GPP data into a 0.05° × 0.05° spatial resolution using the nearest neighbor resampling method to match the satellite observation data.

2.4. Land Vegetated Area Data

The global land use change data obtained from the HIstoric Land Dynamics Assessment+ (HILDA+) project were used to determine China's vegetated regions (Winkler et al., 2021). To focus on our goals, we ignored the transformation between vegetated and non-vegetated regions, thereby reducing the effect of land cover change on vegetation growth. That is, we used the intersection of all the vegetation layers to ensure that each grid cell was a vegetated region from the beginning to the end for the 1982–2015 period. Finally, the China vegetation cover map was aggregated to a 0.05° × 0.05° spatial resolution using the nearest neighbor resampling method to match the satellite observation data.

2.5. Gridded Water Availability Indices

The PDSI, calculated with temperature and precipitation data, is widely used to estimate relative dryness. A PDSI value > 4 represents very wet conditions, while a PDSI < −4 represents an extreme drought. The global monthly PDSI data with a $0.05° \times 0.05°$ spatial resolution were provided by the TerraClimate high-spatial-resolution climate data set (Abatzoglou et al., 2018). The SPEI and TWS data as complementary water availability indices were used to evaluate the robustness of the results based on PDSI. The SPEI03 data obtained from SPEIbase (Version 2) (Vicente-Serrano et al., 2010), representing the 3-month cumulative water balance, were widely used to study the relationship between vegetation growth and drought events (Au et al., 2022; Jiang et al., 2019; Jiao et al., 2021; Wu et al., 2017). We used SPEI03 to reduce the uncertainty associated with the fixed time-scale water availability index. The TWS data were obtained from the global hydrological model, WaterGAP (Version 2.2 d) (Döll et al., 2014). The Aridity Index (AI) obtained from Zomer et al. (2022), was used to identify arid, semi-arid, sub-humid, and humid zones in China. The SPEI and AI data were resampled into a $0.05° \times 0.05°$ spatial resolution using the nearest neighbour resampling method to match the satellite observation data.

2.6. Forcing Data Sets

We obtained the monthly gridded climate data with a $0.05° \times 0.05°$ spatial resolution from the TerraClimate high-spatial-resolution climate data set (Abatzoglou et al., 2018), including air temperature (Tmp), precipitation (Pre), vapor pressure deficit (VPD), downward surface shortwave radiation (Rad), and soil moisture (SM). The monthly gridded atmospheric carbon dioxide (CO_2) data, that is, CO_2 dry mole fractions, were provided by the European Center for Medium-Range Weather Forecasts (ECMWF). We categorized climate factors as "climate" and atmospheric CO_2 as "CO_2," respectively. The CO_2 data were resampled into a $0.05° \times 0.05°$ spatial resolution using the nearest neighbor resampling method to match the other gridded climate data.

2.7. Trend Analysis

To examine the greening of China's vegetated regions, we used the Theil-Sen estimator with the non-parametric Mann-Kendall test to estimate the linear trends of NDVI/LAI/GPP for each grid cell during the 34 active growing seasons (i.e., April–October in each year) from 1982 to 2015. Compared to the fixed growing season described above, we recalculated the trends in NDVI/LAI/GPP for each grid cell based on their maximum growing-season values to reduce the effect of changes in growing-season length. The Theil-Sen estimator with the non-parametric Mann-Kendall test was also used to calculate the trends of the relationship between vegetation growth and water availability over 25 consecutive 10-year moving windows spanning from 1982 to 2015 (i.e., 1982–1991, 1983–1992, …, 2006–2015). The trends in eddy-covariance flux tower-based GPP at the nine sites were calculated by the simple linear regression method. In addition, we used the simple linear regression method to calculate the trends in the climate-, CO_2−, and "other factors"-dominated area across different water constraints.

2.8. Correlation Analysis

To examine vegetation growth responses to water availability, we evaluated the relationship between NDVI/LAI/GPP and PDSI for the 34 active growing seasons during the 1982–2015 period. The Spearman's rank correlation coefficient (r-value) between NDVI/LAI/GPP and PDSI was used to represent the relationship between vegetation growth and water availability. A significant positive correlation coefficient (two-tailed t-test: $p < 0.05$) between NDVI/LAI/GPP and PDSI is interpreted as vegetation growth being constrained by water deficit. Conversely, a significant negative correlation coefficient (two-tailed t-test: $p < 0.05$) suggests that vegetation growth is constrained by water surplus. The grid cells with non-significant correlation coefficients indicate that vegetation growth is not clearly constrained by water availability. For vegetation growth under water deficit, vegetation growth is increasing with wetting and decreasing with drying. Water stress such as drought can limit vegetation growth. For vegetation growth under water surplus, vegetation is less productive under wetter conditions and more productive under drier-than-normal conditions. Water surplus can limit vegetation growth as a result of waterlogging or insufficient temperature and solar radiation due to excessive rainfall. Here, we refer to those grid cells exhibiting significant positive and significant negative correlation coefficients (two-tailed t-test: $p < 0.05$) as "vegetation water deficit regions" and "vegetation water surplus regions," respectively (Jiao et al., 2021). To further decouple the effects of water availability and climate change on vegetation growth, we divided the significant r-value between NDVI/LAI/GPP and PDSI for the 34 active growing seasons into six bins

(i.e., $r \leq -0.5$, $-0.5 < r \leq -0.4$, $-0.4 < r \leq -0.3$, $0.4 > r \geq 0.3$, $0.5 > r \geq 0.4$, and $r \geq 0.5$), and the non-significant part (i.e., $-0.3 < r < 0.3$) was excluded (Liu et al., 2020). In addition, to reduce the effects of the long-term NDVI/LAI/GPP trends and the growing-season length changes, we recalculated the correlation coefficients of the detrended, the maximum, and the detrended maximum NDVI/LAI/GPP with PDSI. We also used SPEI03 as an alternative water availability indicator to further evaluate the robustness of our PDSI-based results (Vicente-Serrano et al., 2013).

2.9. Attribution Analysis

To further reveal the implications of recent water constraints for changes in vegetation growth across China over the past three decades, we evaluated the importance of climate and atmospheric CO_2 for vegetation growth using a partial correlation algorithm (Jiao et al., 2021). The factor with the highest absolute value of the significant partial correlation coefficient (two-tailed t-test: $p < 0.05$) was identified as the dominant driver of vegetation growth in that grid cell (Jiao et al., 2021). We analyzed the partial correlation of NDVI/LAI/GPP with one of those forcing factors (i.e., air temperature, precipitation, vapor pressure deficit, downward surface shortwave radiation, soil moisture, and atmospheric CO_2) by excluding the effects of the other forcing factors. The two climate change-related categories, "climate" and "CO_2," were used to investigate potential shifts in their importance for vegetation growth across different water constraints. We categorized the climate-related factors as "climate" to avoid differences in data or methods that could lead to differences in attributing these climate factors as the primary drivers of vegetation growth. Land use change, nitrogen deposition, forest management, grazing, changes in cultivation practices and varieties, irrigation, extreme events, and so on were considered in an additional category, "other factors" (Zhu et al., 2016). Moreover, to test the robustness of our partial correlation analysis, we employed random forest (RF) models to gauge the dominance of climate and atmospheric CO_2 on NDVI/LAI/GPP. We used the function "TreeBagger" in MATLAB R2023a software (The MathWorks, Inc., Natick, MA, USA) to create the RF models. The "numTrees" parameter was set to "200" to meet our requirements for accuracy and robustness. The RF models were trained pixel by pixel, and then the dominant driver for each grid cell was extracted by ranking the feature importance. This approach is widely recognized for its effectiveness in mitigating the mixing effect of the "other factors" category via nonlinear modeling (Hutley et al., 2022). Furthermore, we performed another analysis using different TRENDYv8 simulation scenarios to reinforce our satellite-based findings. The GPP outputs derived from the S0, S1, S2, and S3 simulation runs were used to isolate the effects of climate and atmospheric CO_2 on vegetation growth (Fernandez-Martinez et al., 2019; Friedlingstein et al., 2019; Obermeier et al., 2021). We defined the trends in simulated GPP derived from S1 minus S0 (S1−S0), S2 minus S1 (S2−S1), and S3 minus S2 minus S1 (S3−S2−S1) as being driven by the "climate," "CO_2," and "other factors" categories, respectively. The category with the highest absolute value of these trends was considered to be the dominant driver of vegetation growth in that grid cell. Overall, we used the three attribution analyses for cross-validation with the aim of reinforcing the robustness of our core findings.

3. Results and Discussion

3.1. Widespread Greening of China's Vegetated Regions Over the Past Three Decades

Here we employed the Theil-Sen estimator in conjunction with the non-parametric Mann-Kendall test to assess the changes in NDVI, LAI, and GPP (hereinafter referred to as "NDVI/LAI/GPP") for each grid cell across China's vegetated regions over the course of 34 active growing seasons (i.e., a fixed time period from April to October each year) from 1982 to 2015. We found that 79.93%, 83.57%, and 65.42% of vegetated grid cells exhibited an increase in NDVI/LAI/GPP during this period (51.49%, 63.31%, and 29.95% with a significant increase, Mann-Kendall test: $p < 0.05$) (Figures 1a–1c). The NDVI, LAI, and GPP-based results showed comparable spatiotemporal patterns of vegetation growth across China over the past three decades. The relative frequency distributions of the various trends were similar. However, we also found some differences in the trends derived from different vegetation growth proxies (Figure S1 in Supporting Information S1). Considering that NDVI, LAI, and GPP represent different vegetation characteristics (e.g., greenness, cover, and productivity), their asynchronous changes in some regions may present different estimates of vegetation growth trends when using them as proxies (Ding et al., 2020; Piao et al., 2019; Zhang et al., 2017). To ensure the reliability of our satellite-based analysis, we incorporated available eddy-covariance flux tower-based GPP data to validate our results (Figure 1d). Seven out of the nine sites experienced an increase in GPP (two sites with a significant increase, two-tailed t-test: $p < 0.05$). In contrast, only two sites exhibited a non-significant decrease in GPP (two-tailed t-test:
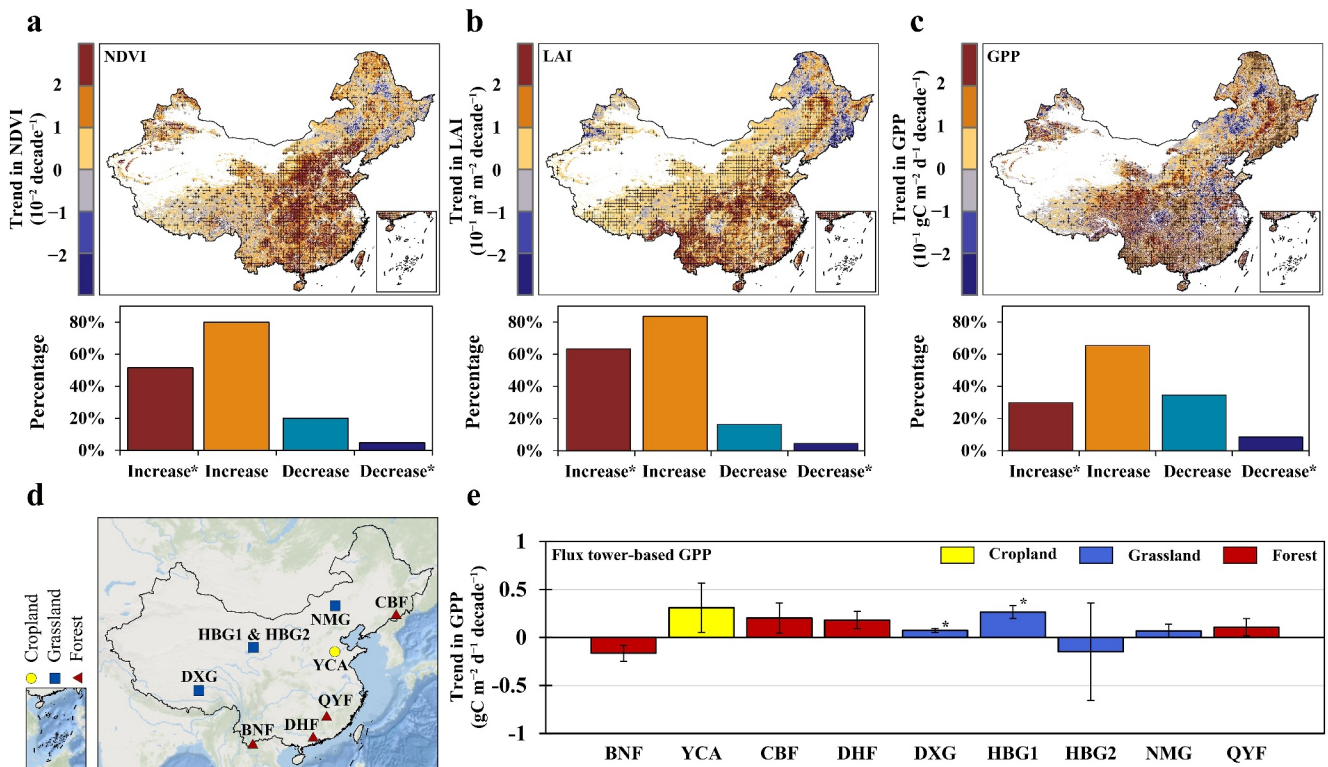
Figure 1. Spatiotemporal patterns of vegetation growth across China over the past three decades. (a–c) Spatial distribution of the trends in the Normalized Difference Vegetation Index (NDVI), Leaf Area Index (LAI), and Gross Primary Productivity (GPP) across China over the 1982–2015 period. The black crosses in panels (a–c) indicate a significant trend with $p < 0.05$ (Mann-Kendall test). The bar charts in panels (a–c) show the relative frequency distribution of significant increases (Mann-Kendall test: $p < 0.05$), increases, decreases, and significant decreases (Mann-Kendall test: $p < 0.05$). (d) Spatial distribution of the nine eddy-covariance flux towers in China. e Trends in eddy-covariance flux tower-based GPP at the nine sites (*, two-tailed t-test: $p < 0.05$). The error bars in (e) show the standard deviation of the trends in GPP derived from a simple linear regression method. BNF: Xishuangbanna (forest, 2003–2010), YCA: Yucheng (cropland, 2003–2010), CBF: Changbaishan (forest, 2003–2010), DHF: Dinghushan (forest, 2003–2010), DXG: Damxung (grassland, 2004–2010), HBG1: Haibei (grassland, 2003–2010), HBG2: Haibei (grassland, 2004–2009), NMG: Inner Mongolia (grassland, 2003–2010), QYF: Qianyanzhou (forest, 2003–2010).

$p > 0.05$) (Figure 1e). To further validate our analysis based on the fixed growing season shown above, we recalculated the trends in NDVI/LAI/GPP for each grid cell based on their maximum growing-season values as indicators of vegetation growth (Figure S2 in Supporting Information S1). Importantly, the widespread greening of China's vegetated regions has been confirmed, regardless of whether we used mean or peak growing-season NDVI/LAI/GPP values to characterize vegetation growth for each year. In addition, we also incorporated the simulated GPP data derived from three widely used DGVMs with a fine spatial resolution, ORCHIDEE (Krinner et al., 2005), SDGVM (Walker et al., 2017), and VISIT (Kato et al., 2013), as part of the TRENDY v8 project (Friedlingstein et al., 2019). The GPP data employed herein was run under the S3 simulation scenario (observed climate and CO_2 and land use/land cover, close to historical conditions). These simulated GPP results consistently affirmed that vegetation growth has increased in most of China's vegetated regions during the study period, whether based on the mean (Figure S3 in Supporting Information S1) or peak (Figure S4 in Supporting Information S1) growing-season values. Overall, whether using satellite and in-situ observations or model-simulated data, multiple lines of evidence confirm that China's vegetation growth has been broadly enhanced over the past three decades. This is also in line with an overall trend of greening of the Earth, as noted in previous studies (Chen et al., 2019; Cortés et al., 2021; Piao et al., 2020; Zhu et al., 2016).

3.2. Spatiotemporal Patterns of the Relationship Between Vegetation Growth and Water Availability

While we observed widespread increases in NDVI/LAI/GPP across China over the past three decades, such a surge in vegetation growth is anticipated to place greater demands on terrestrial water resources (Liu et al., 2023; Yang, Roderick, et al., 2023), leading to increasing water constraints on ecosystems in regions with limited water availability. To delineate vegetation-associated water deficit and water surplus regions in China, we conducted an
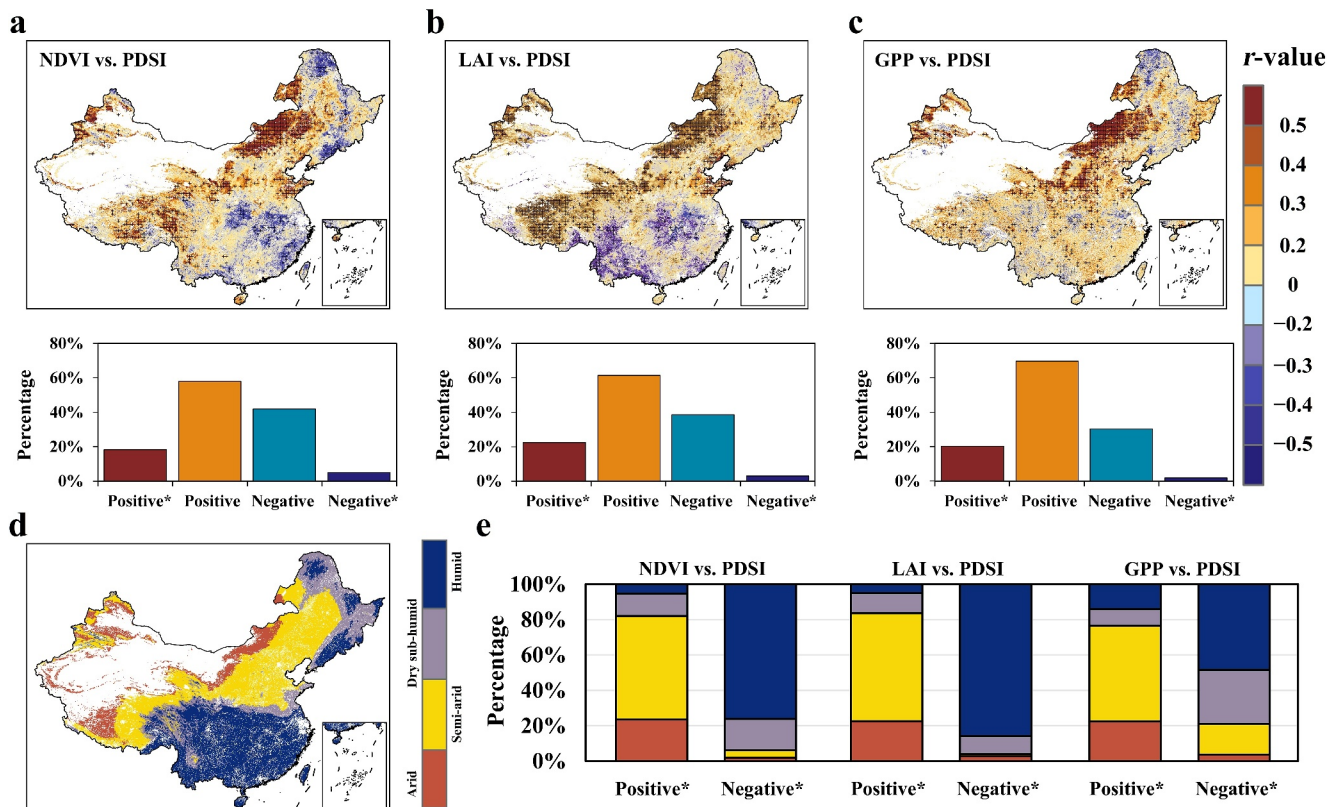
Figure 2. Spatial distribution of the relationship between vegetation growth and water availability across China over the past three decades. (a–c) Spatial distribution of the Spearman's rank correlation coefficient (r-value) between the Normalized Difference Vegetation Index (NDVI)/Leaf Area Index (LAI)/Gross Primary Productivity (GPP) and the Palmer Drought Severity Index (PDSI) across China over the 1982–2015 period. The black crosses in panels (a–c) indicate a significant r-value with $p < 0.05$ (two-tailed t-test). The bar charts in panels (a–c) show the relative frequency distribution of significant positive (two-tailed t-test: $p < 0.05$), positive, negative, and significant negative (two-tailed t-test: $p < 0.05$) correlations. (d) Spatial distribution of arid, semi-arid, dry sub-humid, and humid zones in China according to the Aridity Index (AI). (e) Statistical distribution of the significant correlations between NDVI/LAI/GPP and PDSI (two-tailed t-test: $p < 0.05$) across climate zones colored according to (d).

assessment of the relationship between vegetation growth and water availability for each grid cell during the 34 active growing seasons spanning from 1982 to 2015. We refer to the areas exhibiting significant positive and significant negative Spearman's rank correlation coefficient (r-value) (two-tailed t-test: $p < 0.05$) between NDVI/LAI/GPP and PDSI as "vegetation water deficit regions" and "vegetation water surplus regions," respectively (Jiao et al., 2021). This approach allows us to examine the spatiotemporal patterns of water constraints on vegetation growth across China over the past three decades.

The spatial distribution of the relationship between NDVI/LAI/GPP and PDSI showed that more than half of China's vegetated regions were under water constraints. Specifically, 58.03%, 61.36%, and 69.65% of vegetated grid cells exhibited a positive correlation between NDVI/LAI/GPP and PDSI (18.26%, 22.40%, and 20.31% with a significant correlation coefficient, two-tailed t-test: $p < 0.05$) (Figures 2a–2c). Meanwhile, 5.05%, 2.95%, and 1.78% of vegetated grid cells showed a significant negative correlation (two-tailed t-test: $p < 0.05$). Since the trends in NDVI, LAI and GPP as well as their sensitivities to water availability may be different, our results showed differences in some regions (Figure S5 in Supporting Information S1). Despite this, our NDVI-, LAI-, and GPP-based findings were comparable in general. We also found that the regions with vegetation water deficits (i.e., the areas with a significant positive correlation coefficient) were predominantly situated in arid, semi-arid, and dry sub-humid zones (Figure 2d). Specifically, 95%, 95%, and 86% of the vegetation water deficit regions were located within China's drylands where the AI was less than 0.65, aligning with the expectation that droughts can constrain vegetation growth (Figure 2e). To corroborate our above analysis, we examined the spatial distribution of the relationship between NDVI/LAI/GPP and PDSI using additional analyses. The results based on detrended, maximum, and detrended maximum NDVI/LAI/GPP values were consistent with those derived from
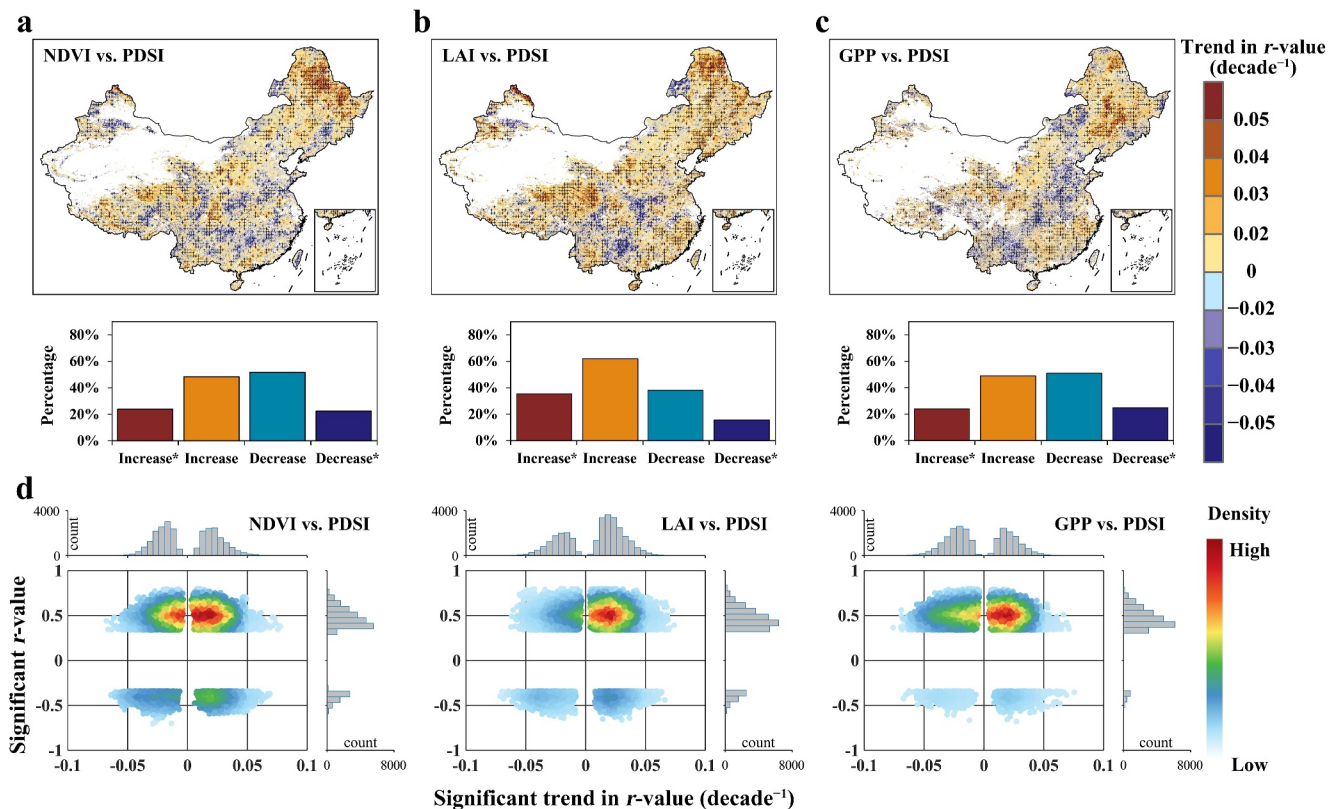
Figure 3. Spatiotemporal patterns of the relationship between vegetation growth and water availability across China over the past three decades. (a–c) Spatial distribution of the trends in the Spearman's rank correlation coefficient (*r*-value) between the Normalized Difference Vegetation Index (NDVI)/Leaf Area Index (LAI)/Gross Primary Productivity (GPP) and Palmer Drought Severity Index (PDSI) for the 25 10-year moving windows across China over the 1982–2015 period. The black crosses in panels (a–c) indicate a significant trend with $p < 0.05$ (Mann-Kendall test). The bar charts in panels (a–c) show the relative frequency distribution of significant increases (Mann-Kendall test: $p < 0.05$), increases, decreases, and significant decreases (Mann-Kendall test: $p < 0.05$). (d) Scatter plots of the significant *r*-value between NDVI/LAI/GPP and PDSI for the entire study period (two-tailed *t*-test: $p < 0.05$) versus the significant trend of the *r*-value between NDVI/LAI/GPP and PDSI for the 25 10-year moving windows (Mann-Kendall test: $p < 0.05$). The histograms in panel (d) represent the count of grid cells on each axis.

non-detrended analysis using the mean growing-season values (Figure S6 in Supporting Information S1). This demonstrated that the relationship between vegetation growth and water availability was not influenced by long-term trends in NDVI/LAI/GPP or variations in growing-season length. In addition, we employed SPEI03 and TWS as alternative indicators of water availability in place of PDSI. The SPEI03- and TWS-based results showed similar patterns to those derived from PDSI (Figure S7 in Supporting Information S1). Taken together, these findings underscore the presence of numerous vegetation water deficit regions, revealing different water constraints on vegetation growth hidden within the greening of China over the past three decades.

Moreover, we tracked the evolving trends in the relationship between vegetation growth and water availability over 25 consecutive 10-year moving windows spanning from 1982 to 2015 (i.e., 1982–1991, 1983–1992,…, 2006–2015). The outcomes revealed that 48.35%, 61.93%, and 49.02% of vegetated grid cells exhibited an increase in the correlation coefficient between NDVI/LAI/GPP and PDSI (23.93%, 35.41%, and 23.97% with a significant increase, Mann-Kendall test: $p < 0.05$) (Figures 3a–3c). Conversely, 51.65%, 38.07%, and 50.98% of vegetated grid cells experienced a decrease (22.43%, 15.61%, and 24.83% with a significant decrease, Mann-Kendall test: $p < 0.05$). The regions where the correlation coefficient between NDVI/GPP and PDSI increased were roughly equivalent in size to those where it decreased, whereas more regions exhibited an increase in the correlation coefficient between LAI and PDSI. NDVI, GPP, and LAI appear to be asynchronous in proxying vegetation growth in response to water constraints (Gupta et al., 2020; Li, Pacheco-Labrador, et al., 2023). Considering NDVI, GPP, and LAI represent different characteristics associated with vegetation growth, the differences between their results are acceptable (Chang et al., 2023; Wagle et al., 2014; Wang, Zhang, et al., 2020; Xie et al., 2019). However, these differences in detail suggest that using only one or two of NDVI, LAI, GPP as

proxies for vegetation growth may lead to misunderstanding of the results. The comparison of the different results derived from NDVI, LAI, GPP data is shown in Figure S8 in Supporting Information S1. Further analysis revealed that approximately half of the vegetation water deficit regions had a significant increase in the correlation coefficient, while the other half had a significant decrease (Figure 3d). The regions showing both increasing and decreasing water constraints exhibited comparable trends over the past three decades, particularly within China's vegetation water deficit regions. Consequently, not all regions have witnessed an increasing water constraint on vegetation growth in China, as previously anticipated (Denissen et al., 2022; Feng & Fu, 2013; Huang et al., 2016; Li et al., 2021). Regional wetting and human interventions may be mitigating water stress in plants (Abel et al., 2023; Li, Pacheco-Labrador, et al., 2023; Liu et al., 2023). Alternatively, rising atmospheric CO_2 concentrations are expected to increase the water use efficiency of plants in vegetation water deficit regions (Donohue et al., 2013; Lu et al., 2016). By counting for year-to-year changes in area, we found that China's water deficit regions underwent cycles of contraction and expansion in terms of their spatial extent (Figure S9 in Supporting Information S1). The occurrence of climate phenomena (e.g., El Niño-Southern Oscillation, ENSO) and the update of government policies may explain these cyclical variations in water constraints on vegetation growth. To affirm the robustness of our above findings, we also took into account the effects of long-term trends in NDVI/LAI/GPP and variations in growing-season length on the analysis (Figure S10 in Supporting Information S1). Besides, we employed SPEI03 and TWS as alternative indicators of water availability instead of PDSI to validate our results (Figure S11 in Supporting Information S1). These findings exhibited consistent patterns with those derived from mean growing-season NDVI/LAI/GPP values with PDSI. Overall, our findings imply that different water constraints on vegetation growth may introduce further uncertainty to China's sustainable vegetation greening trends.

3.3. Implications of Different Water Constraints for Vegetation Growth Trends

Determining whether different water constraints can mediate vegetation growth trends across China over the past three decades is a key motivation of this analysis. To do this, we divided the significant correlation coefficients between vegetation growth and water availability (i.e., the significant positive and negative correlation coefficients between NDVI/LAI/GPP and PDSI, two-tailed t-test: $p < 0.05$) into six bins (i.e., $r \leq -0.5$, $-0.5 < r \leq -0.4$, $-0.4 < r \leq -0.3$, $0.4 > r \geq 0.3$, $0.5 > r \geq 0.4$, and $r \geq 0.5$). These bins represent different water constraints on vegetation growth, including water surpluses and water deficits, allowing us to decouple the effect of water constraints on changes in NDVI/LAI/GPP. The area of the six bins accounted for 0.14%–0.44%, 0.63%–2.09%, 0.99%–2.52%, 4.90%–5.74%, 6.36%–7.26%, and 6.79%–7.94% of the total vegetated area, respectively (Table S1 in Supporting Information S1). By comparison, we found a large number of statistically significant differences between the NDVI/LAI/GPP trends across vegetation water deficit regions (ANOVA test: $p < 0.005$), but almost none across vegetation water surplus regions (ANOVA test: $p > 0.1$) (Figure 4). The regions with more water constraints had smaller trends in vegetation growth. Conversely, water surpluses did not explain the differences in most NDVI/LAI/GPP trends. That is, water deficits played a vital role in slowing down vegetation growth across China during the peroid, making any potential vegetation greening trends dependent on more water availability (Chen et al., 2019; Denissen et al., 2022; Zhu et al., 2016).

Further analysis was conducted to examine potential shifts in the dominant driver of two climate change-related categories, defined as "climate" and "CO_2," on vegetation growth across different water constraints in China over the past three decades. Land use change, nitrogen deposition, forest management, grazing, changes in cultivation practices and varieties, irrigation, extreme events, and so on were considered in an additional category, "other factors" (Zhu et al., 2016). The factor with the highest absolute value of the significant partial correlation coefficient (two-tailed t-test: $p < 0.05$) was identified as the dominant driver of changes in vegetation growth in that grid cell (Jiao et al., 2021). Our results showed a similar spatial pattern of the dominant driver on NDVI/LAI/GPP (Figures 5a–5c). More than 70% of vegetated grid cells were able to be explained by those factors in the "climate" and "CO_2" categories (Figure S12 and Table S2 in Supporting Information S1). Moreover, we explored the area changes in climate-dominated and CO_2-dominated regions across those bins. Our results indicated that the regions with more water constraints have larger areas dominated by "climate" and smaller areas dominated by "CO_2" (Figure 5d and Table S3 in Supporting Information S1). As water constraints increased, the area dominated by "climate" expanded significantly, while that dominated by "CO_2" shrank sharply. The smallest climate-dominated area and the largest CO_2-dominated area were almost both found in the mildest vegetation water surplus bin (i.e., the third bin, $-0.4 < r \leq -0.3$). Those CO_2-dominated regions are likely to depend more on the
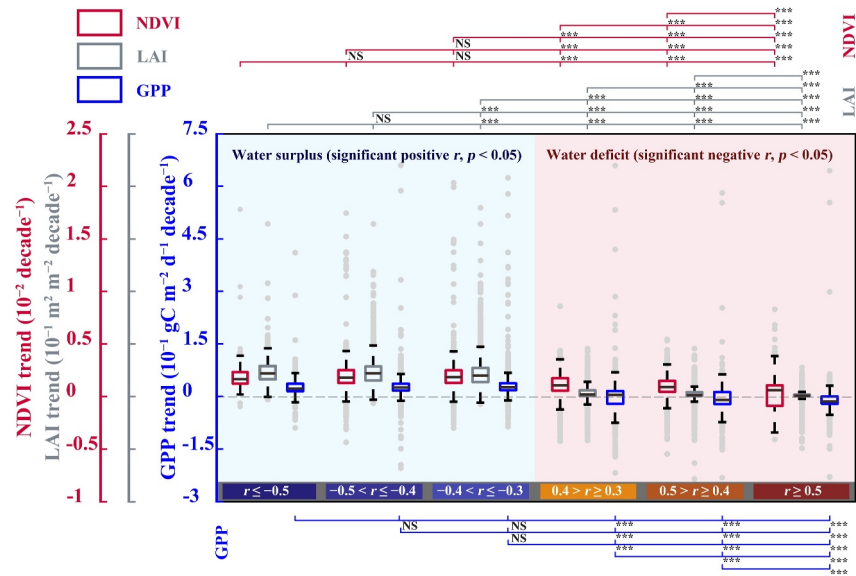
Figure 4. Statistical differences in vegetation growth trends under different water constraints in China over the past three decades. The six bins represent the significant Spearman's rank correlation coefficient (r-value) between the Normalized Difference Vegetation Index (NDVI)/Leaf Area Index (LAI)/Gross Primary Productivity (GPP) and the Palmer Drought Severity Index (PDSI) for the 1982–2015 period, that is, $r \leq -0.5$, $-0.5 < r \leq -0.4$, $-0.4 < r \leq -0.3$, $0.4 > r \geq 0.3$, $0.5 > r \geq 0.4$, and $r \geq 0.5$. *** indicates that the differences between NDVI/LAI/GPP trends are statistically significant (ANOVA test: $p < 0.005$), and NS indicates that the differences are not statistically significant (ANOVA test: $p > 0.1$). The cool and warm colors in panel (d) represent the bins associated with water surpluses and water deficits, respectively.
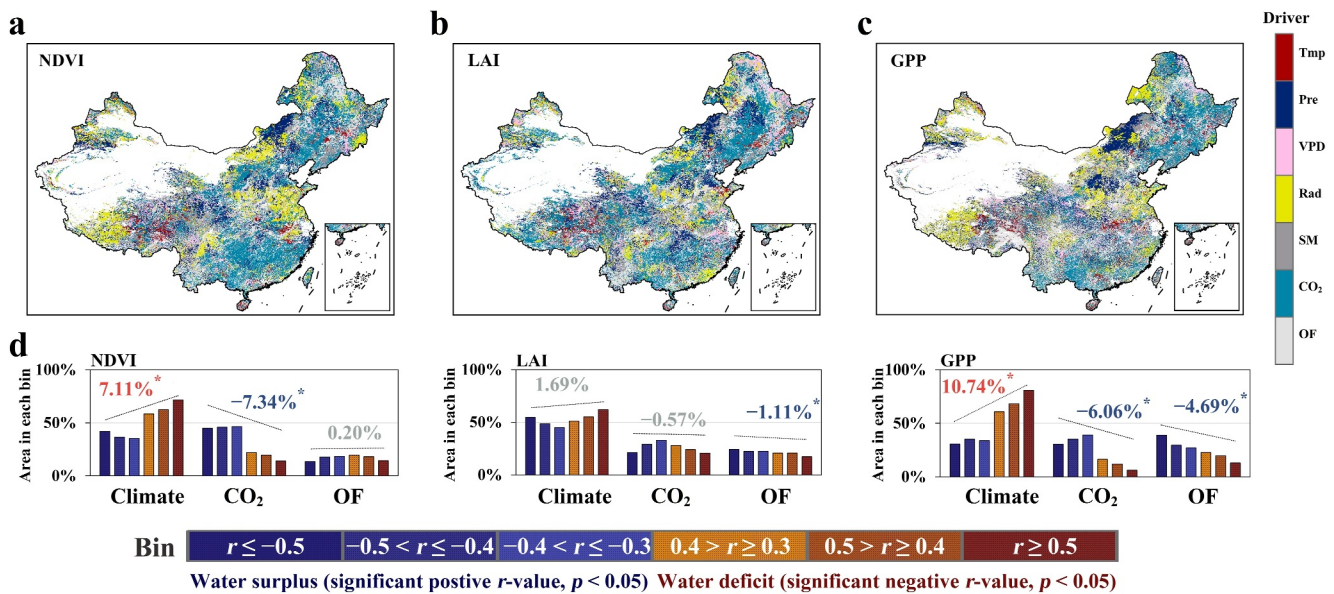

Figure 5. Spatial distribution of the dominant driver on vegetation growth across China over the past three decades. (a–c) Spatial distribution of the dominant driver influencing the Normalized Difference Vegetation Index (NDVI)/Leaf Area Index (LAI)/Gross Primary Productivity (GPP) across China over the 1982–2015 period. The drivers include air temperature (Tmp), precipitation (Pre), vapor pressure deficit (VPD), downward surface shortwave radiation (Rad), soil moisture (SM), atmospheric carbon dioxide (CO_2), and other factors (OF). Land use change, nitrogen deposition, management practices, and so on were considered in the "OF" category. (d) The percentage areas where NDVI/LAI/GPP can be dominated by climate, CO_2, and OF in each bin. The dashed lines in panel (d) show the trends in the climate-, CO_2-, and OF-dominated area across the bins. * in panel (d) indicates a statistically significant trend (two-tailed t-test: $p < 0.05$). The cool and warm colors in panel (d) represent the bins associated with water surpluses and water deficits, respectively.

optimal water supply, reducing in size when environmental conditions are close to "too dry" or "too wet" (Bastos et al., 2019; Fernandez-Martinez et al., 2019; Obermeier et al., 2017; Reich et al., 2014). Considering the sensitivities of NDVI, LAI, and GPP to the forcing factors were different, their results were not completely the same but were similar and comparable. The comparison of the different results derived from NDVI, LAI, GPP data is shown in Figure S13 in Supporting Information S1.

To evaluate the reliability of our partial correlation analysis, we employed the RF models to gauge the dominance of climate and atmospheric CO_2 on NDVI/LAI/GPP across China over the past three decades (Figure S14 in Supporting Information S1). RF models can estimate nonlinear interactions between variables and are relatively insensitive to outliers. We trained RF models pixel by pixel and then extracted the dominant driver for each grid cell by ranking the feature importance. Likewise, the area fraction of climate-dominated and CO_2-dominated regions in China was also contingent on the defined bins, that is, on different water constraints. The smallest climate-dominated area and the largest CO_2-dominated area both persisted within the $-0.4 < r \leq -0.3$ range. Our RF-based findings corroborated those obtained earlier using the partial correlation algorithm. In addition, we performed another analysis using different TRENDYv8 simulation scenarios to reinforce our findings. We assumed that land use/land cover was the most significant driver of vegetation growth in the "other factors" category (Chen et al., 2019; Piao et al., 2020; Zhu et al., 2016). We calculated the trends in simulated GPP under varying CO_2 concentrations, varying climate conditions, and both (Figure S15 in Supporting Information S1). The trends in simulated GPP derived from S1 minus S0 (S1−S0), S2 minus S1 (S2−S1), and S3 minus S2 minus S1 (S3−S2−S1) were considered to be dominated by the "climate," "CO_2," and "other factors" categories, respectively. The category with the highest absolute value of these trends was identified as the dominant driver of vegetation growth in that grid cell. Similarly to our aforementioned methods, we likewise divided the significant correlation coefficient between GPP and PDSI for the 34 active growing seasons into six bins to represent different water constraints on vegetation growth (Figure S16 in Supporting Information S1). However, we found strong inconsistencies in the multi-scenario modeling simulation-based results (Figure S17 in Supporting Information S1). Only the ORCHIDEE model was able to support the results of the other two methods, while the SDGVM and VISIT models exhibited ambiguous patterns of climate- and CO_2-dominated area changes under different water constraints. Overall, given the fact that we should focus more on the similarities between the results derived from different data and methods, this study used three different methods to achieve the attribution analysis for the purpose of minimizing the uncertainty associated with using only one or two approaches. The percentage areas where NDVI/LAI/GPP dominated by climate, CO_2, and OF in each bin are comparable across the three different methods. The spatial patterns of the dominant driver influencing NDVI/LAI/GPP are also similar in general, especially for the results derived from the partial correlation- and machine learning-based methods.

4. Conclusions

In summary, we demonstrated that water constraints can mediate the dominance of climate and atmospheric CO_2 on vegetation growth across China over the past three decades. Consistent with previous studies (Chen et al., 2019; Piao et al., 2015), we found that China's vegetation growth has seen a widespread increase during the period. However, our findings showed that recent water constraints on vegetation growth were hidden in the overall greening of China. More than half of China's vegetated areas were regarded as vegetation water deficit regions, with this situation being expected to worsen in the future (Denissen et al., 2022; Feng & Fu, 2013; Jiao et al., 2021). More importantly, our study revealed that climate and atmospheric CO_2 had different weights in regulating vegetation growth across water deficit and water surplus regions. The proportion of the climate- and atmospheric CO_2-dominated area has varied depending on different water constraints. Despite the fact that previous studies have more often than not attributed vegetation greening trends to land use/land cover change (Chen et al., 2019; Piao et al., 2015; Zhu et al., 2016), climate change remains a non-negligible force influencing vegetation growth. By placing those non-climate change drivers into the "other factors" category, this study focused as much as possible on the implications of recent water constraints for climate change-driven trends in vegetation growth. Overall, our findings are important for further understanding of China's land carbon sink under climate change, highlighting the need for explicit consideration of water constraints on sustainable vegetation greening trends. As an indirect climate change impact, water constraints on vegetation growth should be considered by land surface models to reduce uncertainties in terrestrial water and CO_2 flux projections. The next challenge is to quantify the sensitivities of NDVI, LAI, and GPP to water availability through a plant

physiological perspective for further understanding the mechanisms behind the differences in their responses to water constraints. For decision-makers, it is important to consider spatiotemporal patterns of water constraints on vegetation growth for land use policy and food security.

Conflict of Interest

The authors declare no conflicts of interest relevant to this study.

Data Availability Statement

The GIMMS NDVI data set is available in Vermote ([2019](#)). The GLOBMAP LAI data set is available in Liu et al. ([2021](#)). The GPP_{NIRv} data set is available in Wang, Zhang, and Ju ([2020](#)). The eddy-covariance flux tower-based GPP data for the nine ChinaFLUX sites are available in Song et al. ([2021](#)), Zhao et al. ([2021](#)), Wu et al. ([2020](#)), Shi and He ([2021](#)), Zhang et al. ([2019](#), [2020](#)), Hao et al. ([2020](#)), and Dai et al. ([2020](#)), respectively. The TRENDYv8 simulated GPP data are available on request to Professor Stephen Sitch (s.a.sitch@exeter.ac.uk) and Professor Pierre Friedlingstein (p.friedlingstein@exeter.ac.uk), and more details can be found at https://blogs.exeter.ac.uk/trendy. The HILDA + land use change data are available in Winkler et al. ([2020](#)). The PDSI and climate data are available from the TerraClimate data set (Abatzoglou et al., [2018](#)) at https://www.climatologylab.org/terraclimate.html. The SPEI data set is available in Beguería et al. ([2017](#)). The TWS data set is available in Müller Schmied et al. ([2020](#)). The AI data set is available in Zomer and Trabucco ([2019](#)). The monthly gridded atmospheric CO_2 data are available from the Copernicus Atmosphere Monitoring Service (CAMS) at https://ads.atmosphere.copernicus.eu/cdsapp#!/dataset/cams-global-greenhouse-gas-inversion?tab=overview. The data and code that support the findings of this study can be found in the Figshare data repository (Song, [2023a](#), [2023b](#), [2023c](#), [2023d](#)).

References

Abatzoglou, J. T., Dobrowski, S. Z., Parks, S. A., & Hegewisch, K. C. (2018). TerraClimate, a high-resolution global dataset of monthly climate and climatic water balance from 1958-2015. *Scientific Data*, *5*(1), 170191. https://doi.org/10.1038/sdata.2017.191

Abel, C., Abdi, A. M., Tagesson, T., Horion, S., & Fensholt, R. (2023). Contrasting ecosystem vegetation response in global drylands under drying and wetting conditions. *Global Change Biology*, *29*(14), 3954–3969. https://doi.org/10.1111/gcb.16745

Anderegg, W. R. L., Konings, A. G., Trugman, A. T., Yu, K. L., Bowling, D. R., Gabbitas, R., et al. (2018). Hydraulic diversity of forests regulates ecosystem resilience during drought. *Nature*, *561*(7724), 538–541. https://doi.org/10.1038/s41586-018-0539-7

Au, T. F., Maxwell, J. T., Robeson, S. M., Li, J., Siani, S. M. O., Novick, K. A., et al. (2022). Younger trees in the upper canopy are more sensitive but also more resilient to drought. *Nature Climate Change*, *12*, 1168–1174. https://doi.org/10.1038/s41558-022-01528-w

Bastos, A., Ciais, P., Chevallier, F., Rödenbeck, C., Ballantyne, A. P., Maignan, F., et al. (2019). Contrasting effects of CO_2 fertilization, land-use change and warming on seasonal amplitude of Northern Hemisphere CO_2 exchange. *Atmospheric Chemistry and Physics*, *19*, 12361–12375. https://doi.org/10.5194/acp-19-12361-2019

Beguería, S., Vicente-Serrano, S. M., Reig-Gracia, F., & Latorre Garcés, B. (2017). SPEIbase (version 2.5) [Dataset]. *DIGITAL.CSIC*. https://doi.org/10.20350/digitalCSIC/8508

Berg, A., & McColl, K. A. (2021). No projected global drylands expansion under greenhouse warming. *Nature Climate Change*, *11*(4), 331–337. https://doi.org/10.1038/s41558-021-01007-8

Bueso, D., Piles, M., Ciais, P., Wigneron, J.-P., Moreno-Martínez, Á., & Camps-Valls, G. (2023). Soil and vegetation water content identify the main terrestrial ecosystem changes. *National Science Review*, *10*(5), nwad026. https://doi.org/10.1093/nsr/nwad026

Chang, Q., He, H., Ren, X., Zhang, L., Feng, L., Lv, Y., et al. (2023). Soil moisture drives the spatiotemporal patterns of asymmetry in vegetation productivity responses across China. *Science of the Total Environment*, *855*, 158819. https://doi.org/10.1016/j.scitotenv.2022.158819

Chen, C., Park, T., Wang, X., Piao, S., Xu, B., Chaturvedi, R. K., et al. (2019). China and India lead in greening of the world through land-use management. *Nature Sustainability*, *2*, 122–129. https://doi.org/10.1038/s41893-019-0220-7

Ciais, P., Reichstein, M., Viovy, N., Granier, A., Ogee, J., Allard, V., et al. (2005). Europe-wide reduction in primary productivity caused by the heat and drought in 2003. *Nature*, *437*(7058), 529–533. https://doi.org/10.1038/nature03972

Cortés, J., Mahecha, M. D., Reichstein, M., Myneni, R. B., Chen, C., & Brenning, A. (2021). Where are global vegetation greening and browning trends significant? *Geophysical Research Letters*, *48*(6), e2020GL091496. https://doi.org/10.1029/2020GL091496

Dai, X., Wang, H., Xu, M., Yang, F., Wen, X., Chen, Z., et al. (2020). An observation dataset of carbon and water fluxes of artificial coniferous forests in Qianyanzhou (2003–2010) [Dataset]. *Science Data Bank*. https://doi.org/10.11922/sciencedb.993

Denissen, J. M. C., Teuling, A. J., Pitman, A. J., Koirala, S., Migliavacca, M., Li, W. T., et al. (2022). Widespread shift from ecosystem energy to water limitation with climate change. *Nature Climate Change*, *12*(7), 677–684. https://doi.org/10.1038/s41558-022-01403-8

Ding, Z., Peng, J., Qiu, S., & Zhao, Y. (2020). Nearly half of global vegetated area experienced inconsistent vegetation growth in terms of greenness, cover, and productivity. *Earth's Future*, *8*(10), e2020EF001618. https://doi.org/10.1029/2020ef001618

Döll, P., Müller Schmied, H., Schuh, C., Portmann, F. T., & Eicker, A. (2014). Global-scale assessment of groundwater depletion and related groundwater abstractions: Combining hydrological modeling with information from well observations and GRACE satellites. *Water Resources Research*, *50*(7), 5698–5720. https://doi.org/10.1002/2014wr015595

Donohue, R. J., Roderick, M. L., McVicar, T. R., & Farquhar, G. D. (2013). Impact of CO_2 fertilization on maximum foliage cover across the globe's warm, arid environments. *Geophysical Research Letters*, *40*(12), 3031–3035. https://doi.org/10.1002/grl.50563

Feng, S., & Fu, Q. (2013). Expansion of global drylands under a warming climate. *Atmospheric Chemistry and Physics*, *13*(19), 10081–10094. https://doi.org/10.5194/acp-13-10081-2013

Fernandez-Martinez, M., Sardans, J., Chevallier, F., Ciais, P., Obersteiner, M., Vicca, S., et al. (2019). Global trends in carbon sinks and their relationships with CO_2 and temperature. *Nature Climate Change*, *9*(1), 73–79. https://doi.org/10.1038/s41558-018-0367-7

Friedlingstein, P., Jones, M. W., O'Sullivan, M., Andrew, R. M., Hauck, J., Peters, G. P., et al. (2019). Global carbon budget 2019. *Earth System Science Data*, *11*(4), 1783–1838. https://doi.org/10.5194/essd-11-1783-2019

Gerlein-Safdi, C., Keppel-Aleks, G., Wang, F., Frolking, S., & Mauzerall, D. L. (2020). Satellite monitoring of natural reforestation efforts in China's drylands. *One Earth*, *2*(1), 98–108. https://doi.org/10.1016/j.oneear.2019.12.015

Gonsamo, A., Ciais, P., Miralles, D. G., Sitch, S., Dorigo, W., Lombardozzi, D., et al. (2021). Greening drylands despite warming consistent with carbon dioxide fertilization effect. *Global Change Biology*, *27*(14), 3336–3349. https://doi.org/10.1111/gcb.15658

Gupta, A., Rico-Medina, A., & Cano-Delgado, A. I. (2020). The physiology of plant responses to drought. *Science*, *368*(6488), 266–269. https://doi.org/10.1126/science.aaz7614

Hao, Y., Zhang, L., Sun, X., Yu, G., Chen, Z., & Wang, Y. (2020). A dataset of carbon and water fluxes over Xilinhot temperate steppe in Inner Mongolia (2003–2010) [Dataset]. *Science Data Bank*. https://doi.org/10.11922/sciencedb.996

He, B., Wang, S., Guo, L., & Wu, X. (2019). Aridity change and its correlation with greening over drylands. *Agricultural and Forest Meteorology*, *278*, 107663. https://doi.org/10.1016/j.agrformet.2019.107663

Higgins, S. I., Conradi, T., & Muhoko, E. (2023). Shifts in vegetation activity of terrestrial ecosystems attributable to climate trends. *Nature Geoscience*, *16*(2), 147–153. https://doi.org/10.1038/s41561-022-01114-x

Hsu, H., & Dirmeyer, P. A. (2023). Soil moisture-evaporation coupling shifts into new gears under increasing CO_2. *Nature Communications*, *14*(1), 1162. https://doi.org/10.1038/s41467-023-36794-5

Huang, J., Yu, H., Guan, X., Wang, G., & Guo, R. (2016). Accelerated dryland expansion under climate change. *Nature Climate Change*, *6*(2), 166–171. https://doi.org/10.1038/nclimate2837

Huang, Z., Yuan, X., Sun, S., Leng, G., & Tang, Q. (2023). Groundwater depletion rate over China during 1965–2016: The long-term trend and inter-annual variation. *Journal of Geophysical Research: Atmospheres*, *128*(11), e2022JD038109. https://doi.org/10.1029/2022jd038109

Humphrey, V., Zscheischler, J., Ciais, P., Gudmundsson, L., Sitch, S., & Seneviratne, S. I. (2018). Sensitivity of atmospheric CO_2 growth rate to observed changes in terrestrial water storage. *Nature*, *560*(7720), 628–631. https://doi.org/10.1038/s41586-018-0424-4

Hutley, L. B., Beringer, J., Fatichi, S., Schymanski, S. J., & Northwood, M. (2022). Gross primary productivity and water use efficiency are increasing in a high rainfall tropical savanna. *Global Change Biology*, *28*(7), 2360–2380. https://doi.org/10.1111/gcb.16012

Jiang, P., Liu, H., Piao, S., Ciais, P., Wu, X., Yin, Y., & Wang, H. (2019). Enhanced growth after extreme wetness compensates for post-drought carbon loss in dry forests. *Nature Communications*, *10*(1), 195. https://doi.org/10.1038/s41467-018-08229-z

Jiao, W., Wang, L., Smith, W. K., Chang, Q., Wang, H., & D'Odorico, P. (2021). Observed increasing water constraint on vegetation growth over the last three decades. *Nature Communications*, *12*(1), 3777. https://doi.org/10.1038/s41467-021-24016-9

Kato, E., Kinoshita, T., Ito, A., Kawamiya, M., & Yamagata, Y. (2013). Evaluation of spatially explicit emission scenario of land-use change and biomass burning using a process-based biogeochemical model. *Journal of Land Use Science*, *8*(1), 104–122. https://doi.org/10.1080/1747423x.2011.628705

Krinner, G., Viovy, N., de Noblet-Ducoudre, N., Ogee, J., Polcher, J., Friedlingstein, P., et al. (2005). A dynamic global vegetation model for studies of the coupled atmosphere-biosphere system. *Global Biogeochemical Cycles*, *19*(1), GB1015. https://doi.org/10.1029/2003gb002199

Li, C., Fu, B., Wang, S., Stringer, L. C., Wang, Y., Li, Z., et al. (2021). Drivers and impacts of changes in China's drylands. *Nature Reviews Earth & Environment*, *2*(12), 858–873. https://doi.org/10.1038/s43017-021-00226-z

Li, W., Migliavacca, M., Forkel, M., Denissen, J. M. C., Reichstein, M., Yang, H., et al. (2022). Widespread increasing vegetation sensitivity to soil moisture. *Nature Communications*, *13*(1), 3959. https://doi.org/10.1038/s41467-022-31667-9

Li, W., Pacheco-Labrador, J., Migliavacca, M., Miralles, D., Hoek van Dijke, A., Reichstein, M., et al. (2023). Widespread and complex drought effects on vegetation physiology inferred from space. *Nature Communications*, *14*(1), 4640. https://doi.org/10.1038/s41467-023-40226-9

Li, X., Ryu, Y., Xiao, J., Dechant, B., Liu, J., Li, B., et al. (2023). New-generation geostationary satellite reveals widespread midday depression in dryland photosynthesis during 2020 western U.S. heatwave. *Science Advances*, *9*(31), eadi0775. https://doi.org/10.1126/sciadv.adi0775

Li, X., Xiao, J., Kimball, J. S., Reichle, R. H., Scott, R. L., Litvak, M. E., et al. (2020). Synergistic use of SMAP and OCO-2 data in assessing the responses of ecosystem productivity to the 2018 U.S. drought. *Remote Sensing of Environment*, *251*, 112062. https://doi.org/10.1016/j.rse.2020.112062

Li, X., Zhang, Y., Ma, N., Zhang, X., Tian, J., Zhang, L., et al. (2023). Increased grain crop production intensifies the water crisis in Northern China. *Earth's Future*, *11*(9), e2023EF003608. https://doi.org/10.1029/2023ef003608

Liu, K., Li, X., Wang, S., & Zhou, G. (2023). Past and future adverse response of terrestrial water storages to increased vegetation growth in drylands. *npj Climate and Atmospheric Science*, *6*(1), 113. https://doi.org/10.1038/s41612-023-00437-9

Liu, L., Gudmundsson, L., Hauser, M., Qin, D., Li, S., & Seneviratne, S. I. (2020). Soil moisture dominates dryness stress on ecosystem production globally. *Nature Communications*, *11*(1), 4892. https://doi.org/10.1038/s41467-020-18631-1

Liu, Y., Liu, R., & Chen, J. (2012). Retrospective retrieval of long-term consistent global leaf area index (1981-2011) from combined AVHRR and MODIS data. *Journal of Geophysical Research*, *117*(G4), G04003. https://doi.org/10.1029/2012jg002084

Liu, Y., Liu, R., & Chen, J. (2021). GLOBMAP global leaf area index since 1981 [Dataset]. *Zenodo*. https://doi.org/10.5281/zenodo.4700264

Lu, X., Wang, L., & McCabe, M. F. (2016). Elevated CO_2 as a driver of global dryland greening. *Scientific Reports*, *6*(1), 20716. https://doi.org/10.1038/srep20716

Müller Schmied, H., Cáceres, D., Eisner, S., Flörke, M., Herbert, C., Niemann, C., et al. (2020). The global water resources and use model WaterGAP v2.2d – Standard model output [Dataset]. *PANGAEA*. https://doi.org/10.1594/PANGAEA.918447

Novick, K. A., Ficklin, D. L., Stoy, P. C., Williams, C. A., Bohrer, G., Oishi, A. C., et al. (2016). The increasing importance of atmospheric demand for ecosystem water and carbon fluxes. *Nature Climate Change*, *6*(11), 1023–1027. https://doi.org/10.1038/nclimate3114

Obermeier, W. A., Lehnert, L. W., Kammann, C. I., Muller, C., Grunhage, L., Luterbacher, J., et al. (2017). Reduced CO_2 fertilization effect in temperate C3 grasslands under more extreme weather conditions. *Nature Climate Change*, *7*(2), 137–141. https://doi.org/10.1038/nclimate3191

Obermeier, W. A., Nabel, J. E. M. S., Loughran, T., Hartung, K., Bastos, A., Havermann, F., et al. (2021). Modelled land use and land cover change emissions – A spatio-temporal comparison of different approaches. *Earth System Dynamics*, *12*(2), 635–670. https://doi.org/10.5194/esd-12-635-2021

Penuelas, J. (2023). Decreasing efficiency and slowdown of the increase in terrestrial carbon-sink activity. *One Earth*, *6*, 591–594. https://doi.org/10.1016/j.oneear.2023.05.013

Penuelas, J., Ciais, P., Canadell, J. G., Janssens, I. A., Fernandez-Martinez, M., Carnicer, J., et al. (2017). Shifting from a fertilization-dominated to a warming-dominated period. *Nature Ecology & Evolution*, *1*(10), 1438–1445. https://doi.org/10.1038/s41559-017-0274-8

Piao, S., Ciais, P., Huang, Y., Shen, Z., Peng, S., Li, J., et al. (2010). The impacts of climate change on water resources and agriculture in China. *Nature*, *467*(7311), 43–51. https://doi.org/10.1038/nature09364

Piao, S., Wang, X., Park, T., Chen, C., Lian, X., He, Y., et al. (2019). Characteristics, drivers and feedbacks of global greening. *Nature Reviews Earth & Environment*, *1*, 14–27. https://doi.org/10.1038/s43017-019-0001-x

Piao, S., Wang, X., Park, T., Chen, C., Lian, X., He, Y., et al. (2020). Characteristics, drivers and feedbacks of global greening. *Nature Reviews Earth & Environment*, *1*, 14–27. https://doi.org/10.1038/s43017-019-0001-x

Piao, S., Yin, G., Tan, J., Cheng, L., Huang, M., Li, Y., et al. (2015). Detection and attribution of vegetation greening trend in China over the last 30 years. *Global Change Biology*, *21*(4), 1601–1609. https://doi.org/10.1111/gcb.12795

Pinzon, J. E., & Tucker, C. J. (2014). A non-stationary 1981-2012 AVHRR NDVI3g time series. *Remote Sensing*, *6*(8), 6929–6960. https://doi.org/10.3390/rs6086929

Pokhrel, Y., Felfelani, F., Satoh, Y., Boulange, J., Burek, P., Gadeke, A., et al. (2021). Global terrestrial water storage and drought severity under climate change. *Nature Climate Change*, *11*(3), 226–233. https://doi.org/10.1038/s41558-020-00972-w

Reich, P. B., Hobbie, S. E., & Lee, T. D. (2014). Plant growth enhancement by elevated CO_2 eliminated by joint water and nitrogen limitation. *Nature Geoscience*, *7*(12), 920–924. https://doi.org/10.1038/ngeo2284

Sellers, P. J., Dickinson, R. E., Randall, D. A., Betts, A. K., Hall, F. G., Berry, J. A., et al. (1997). Modeling the exchanges of energy, water, and carbon between continents and the atmosphere. *Science*, *275*(5299), 502–509. https://doi.org/10.1126/science.275.5299.502

Sherwood, S., & Fu, Q. (2014). A drier future? *Science*, *343*(6172), 737–739. https://doi.org/10.1126/science.1247620

Shi, P., & He, Y. (2021). An observation dataset of carbon and water fluxes over alpine meadow in Damxung (2004–2010) [Dataset]. *Science Data Bank*. https://doi.org/10.11922/sciencedb.j00001.00248

Smith, T., & Boers, N. (2023). Global vegetation resilience linked to water availability and variability. *Nature Communications*, *14*(1), 498. https://doi.org/10.1038/s41467-023-36207-7

Song, Q., Zhang, Y., Qi, D., Fei, X., Sha, L., Liu, Y., et al. (2021). An observation dataset of carbon and water fluxes in Xishuangbanna tropical seasonal rain forest from 2003 to 2010 [Dataset]. *Science Data Bank*. https://doi.org/10.11922/sciencedb.j00001.00177

Song, Y. (2023a). 1.Spatiotemporal patterns of vegetation growth across China over the past three decades [Dataset]. *Figshare*. https://doi.org/10.6084/m9.figshare.24493528.v1

Song, Y. (2023b). 2.Spatial distribution of the relationship between vegetation growth and water availability across China over the past three decades [Dataset]. *Figshare*. https://doi.org/10.6084/m9.figshare.24494824.v1

Song, Y. (2023c). 3.Spatiotemporal patterns of the relationship between vegetation growth and water availability across China over the past three decades [Dataset]. *Figshare*. https://doi.org/10.6084/m9.figshare.24495130.v1

Song, Y. (2023d). 4. Spatial distribution of the dominant drivers on vegetation growth across China over the past three decades [Dataset]. *Figshare*. https://doi.org/10.6084/m9.figshare.24495238.v1

Song, Y., Jiao, W., Wang, J., & Wang, L. (2022). Increased global vegetation productivity despite rising atmospheric dryness over the last two decades. *Earth's Future*, *10*(7). https://doi.org/10.1029/2021EF002634

Thomas, R. T., Prentice, L. C., Graven, H., Ciais, P., Fisher, J. B., Hayes, D. J., et al. (2016). Increased light-use efficiency in northern terrestrial ecosystems indicated by CO_2 and greening observations. *Geophysical Research Letters*, *43*(21), 11339–11349. https://doi.org/10.1002/2016gl070710

Tong, X., Brandt, M., Yue, Y., Horion, S., Wang, K., De Keersmaecker, W., et al. (2018). Increased vegetation growth and carbon stock in China karst via ecological engineering. *Nature Sustainability*, *1*, 44–50. https://doi.org/10.1038/s41893-017-0004-x

Vermote, E. (2019). NOAA Climate Data Record (CDR) of AVHRR normalized difference vegetation index (NDVI) (Version 5) [Dataset]. *NOAA National Centers for Environmental Information*. https://doi.org/10.7289/V5ZG6QH9

Vicente-Serrano, S. M., Beguería, S., López-Moreno, J. I., Angulo, M., & El Kenawy, A. (2010). A new global 0.5° gridded dataset (1901–2006) of a multiscalar drought index: Comparison with current drought Index datasets based on the Palmer drought severity index. *Journal of Hydrometeorology*, *11*(4), 1033–1043. https://doi.org/10.1175/2010jhm1224.1

Vicente-Serrano, S. M., Gouveia, C., Camarero, J. J., Beguería, S., Trigo, R., Lopez-Moreno, J. I., et al. (2013). Response of vegetation to drought time-scales across global land biomes. *Proceedings of the National Academy of Sciences of the United States of America*, *110*(1), 52–57. https://doi.org/10.1073/pnas.1207068110

Wagle, P., Xiao, X., Torn, M. S., Cook, D. R., Matamala, R., Fischer, M. L., et al. (2014). Sensitivity of vegetation indices and gross primary production of tallgrass prairie to severe drought. *Remote Sensing of Environment*, *152*, 1–14. https://doi.org/10.1016/j.rse.2014.05.010

Walker, A. P., Quaife, T., Bodegom, P. M., De Kauwe, M. G., Keenan, T. F., Joiner, J., et al. (2017). The impact of alternative trait-scaling hypotheses for the maximum photosynthetic carboxylation rate (Vcmax) on global gross primary production. *New Phytologist*, *215*(4), 1370–1386. https://doi.org/10.1111/nph.14623

Wang, L., Jiao, W., MacBean, N., Rulli, M. C., Manzoni, S., Vico, G., & D'Odorico, P. (2022). Dryland productivity under a changing climate. *Nature Climate Change*, *12*(11), 981–994. https://doi.org/10.1038/s41558-022-01499-y

Wang, S., Zhang, Y., & Ju, W. (2020a). Long-term (1982-2018) global gross primary production dataset based on NIRv [Dataset]. *Figshare*. https://doi.org/10.6084/m9.figshare.12981977.v2

Wang, S., Zhang, Y., Ju, W., Chen, J. M., Ciais, P., Cescatti, A., et al. (2020). Recent global decline of CO_2 fertilization effects on vegetation photosynthesis. *Science*, *370*(6522), 1295–1300. https://doi.org/10.1126/science.abb7772

Wang, S., Zhang, Y., Ju, W., Qiu, B., & Zhang, Z. (2021). Tracking the seasonal and inter-annual variations of global gross primary production during last four decades using satellite near-infrared reflectance data. *Science of the Total Environment*, *755*, 142569. https://doi.org/10.1016/j.scitotenv.2020.142569

Wang, X., Xiao, X., Zou, Z., Dong, J., Qin, Y., Doughty, R. B., et al. (2020). Gainers and losers of surface and terrestrial water resources in China during 1989–2016. *Nature Communications*, *11*(1), 3471. https://doi.org/10.1038/s41467-020-17103-w

Wei, X., He, W., Zhou, Y., Cheng, N., Xiao, J., Bi, W., et al. (2023). Increased sensitivity of global vegetation productivity to drought over the recent three decades. *Journal of Geophysical Research-Atmospheres*, *128*(7), e2022JD037504. https://doi.org/10.1029/2022JD037504

Winkler, K., Fuchs, R., Rounsevell, M., & Herold, M. (2020). HILDA+ Global land use change between 1960 and 2019 [Dataset]. *PANGAEA*. https://doi.org/10.1594/PANGAEA.921846

Winkler, K., Fuchs, R., Rounsevell, M., & Herold, M. (2021). Global land use changes are four times greater than previously estimated. *Nature Communications*, *12*(1), 2501. https://doi.org/10.1038/s41467-021-22702-2

Wu, J., Guan, D., Wang, A., Yuan, F., Diao, H., Yu, G., et al. (2020). A dataset of carbon and water flux observation over broad-leaved red pine forest in Changbai Mountain (2003–2010) [Dataset]. *Science Data Bank*. https://doi.org/10.11922/sciencedb.1000

Wu, X., Liu, H., Li, X., Ciais, P., Babst, F., Guo, W., et al. (2017). Differentiating drought legacy effects on vegetation growth over the temperate Northern Hemisphere. *Global Change Biology*, *24*(1), 504–516. https://doi.org/10.1111/gcb.13920

Xie, X., Li, A., Jin, H., Tan, J., Wang, C., Lei, G., et al. (2019). Assessment of five satellite-derived LAI datasets for GPP estimations through ecosystem models. *Science of the Total Environment*, *690*, 1120–1130. https://doi.org/10.1016/j.scitotenv.2019.06.516

Yang, B., Cui, Q., Meng, Y., Zhang, Z., Hong, Z., Hu, F., et al. (2023). Combined multivariate drought index for drought assessment in China from 2003 to 2020. *Agricultural Water Management*, *281*, 108241. https://doi.org/10.1016/j.agwat.2023.108241

Yang, Y., Roderick, M. L., Guo, H., Miralles, D. G., Zhang, L., Fatichi, S., et al. (2023). Evapotranspiration on a greening Earth. *Nature Reviews Earth & Environment*, *4*(9), 626–641. https://doi.org/10.1038/s43017-023-00464-3

Yuan, W., Zheng, Y., Piao, S., Ciais, P., Lombardozzi, D., Wang, Y., et al. (2019). Increased atmospheric vapor pressure deficit reduces global vegetation growth. *Science Advances*, *5*(8), eaax1396. https://doi.org/10.1126/sciadv.aax1396

Zhang, F., Li, H., Zhao, L., Zhang, L., Chen, Z., Zhu, J., et al. (2019). An observation dataset of carbon, water and heat fluxes of alpine shrubland in Haibei (2003–2010) [Dataset]. *Science Data Bank*. https://doi.org/10.11922/sciencedb.1007

Zhang, F., Li, H., Zhao, L., Zhang, L., Chen, Z., Zhu, J., et al. (2020). An observation dataset of carbon, water and heat fluxes of alpine wetland in Haibei (2004–2009) [Dataset]. *Science Data Bank*. https://doi.org/10.11922/sciencedb.1010

Zhang, T., Zhou, J., Yu, P., Li, J., Kang, Y., & Zhang, B. (2023). Response of ecosystem gross primary productivity to drought in northern China based on multi-source remote sensing data. *Journal of Hydrology*, *616*, 128808. https://doi.org/10.1016/j.jhydrol.2022.128808

Zhang, Y., Gentine, P., Luo, X., Lian, X., Liu, Y., Zhou, S., et al. (2022). Increasing sensitivity of dryland vegetation greenness to precipitation due to rising atmospheric CO_2. *Nature Communications*, *13*(1), 4875. https://doi.org/10.1038/s41467-022-32631-3

Zhang, Y., Liu, X., Jiao, W., Wu, X., Zeng, X., Zhao, L., et al. (2023). Spatial heterogeneity of vegetation resilience changes to different drought types. *Earth's Future*, *11*(4), e2022EF003108. https://doi.org/10.1029/2022ef003108

Zhang, Y., Song, C., Band, L. E., Sun, G., & Li, J. (2017). Reanalysis of global terrestrial vegetation trends from MODIS products: Browning or greening? *Remote Sensing of Environment*, *191*, 145–155. https://doi.org/10.1016/j.rse.2016.12.018

Zhao, F., Li, F., Zhan, C., Zhang, L., & Chen, Z. (2021). A carbon and water fluxes dataset over farmland ecosystem of winter wheat and summer corn in Yucheng (2003–2010) [Dataset]. *Science Data Bank*. https://doi.org/10.11922/sciencedb.j00001.20002

Zhao, M., & Running, S. W. (2010). Drought-induced reduction in global terrestrial net primary production from 2000 through 2009. *Science*, *329*(5994), 940–943. https://doi.org/10.1126/science.1192666

Zhu, Z., Piao, S., Myneni, R. B., Huang, M., Zeng, Z., Canadell, J. G., et al. (2016). Greening of the Earth and its drivers. *Nature Climate Change*, *6*(8), 791–795. https://doi.org/10.1038/nclimate3004

Zomer, R. J., & Trabucco, A. (2019). Global aridity index and potential evapotranspiration (ET0) database: Version 3 [Dataset]. *Figshare*. https://doi.org/10.6084/m9.figshare.7504448.v6

Zomer, R. J., Xu, J. C., & Trabucco, A. (2022). Version 3 of the global aridity index and potential evapotranspiration database. *Scientific Data*, *9*(1), 409. https://doi.org/10.1038/s41597-022-01493-1